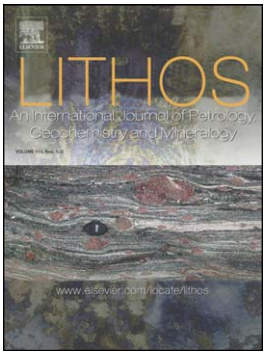

Geochemistry and zircon geochronology of the Permian A-type Hasanrobat granite, Sanandaj-Sirjan belt: A new record of the Gondwana break-up in Iran

Saeed Alirezaei, Jamshid Hassanzadeh

PII: S0024-4937(11)00345-8
DOI: doi: 10.1016/j.lithos.2011.11.015
Reference: LITHOS 2569

To appear in: *LITHOS*

Received date: 14 April 2011
Accepted date: 19 November 2011

Please cite this article as: Alirezaei, Saeed, Hassanzadeh, Jamshid, Geochemistry and zircon geochronology of the Permian A-type Hasanrobat granite, Sanandaj-Sirjan belt: A new record of the Gondwana break-up in Iran, *LITHOS* (2011), doi: 10.1016/j.lithos.2011.11.015

Geochemistry and zircon geochronology of the Permian A-type Hasanrobat granite, Sanandaj-Sirjan belt: a new record of the Gondwana break-up in Iran

Saeed Alirezaei [a], Jamshid Hassanzadeh [b]

[a] Faculty of Earth Sciences, Shahid Beheshti University, Tehran, Iran

[b] Tectonics Observatory, California Institute of Technology, Pasadena, CA 91125, USA

Abstract

The Sanandaj-Sirjan metamorphic-plutonic Belt (SSB) in west central Iran is a polyphase metamorphic terrain composed of dominantly greenschist-grade metasedimentary and metavolcanic rocks, and felsic to mafic plutons, of Neoproterozoic-Phanerozoic ages. The Hasanrobat granite in central SSB occurs as a single pluton, ~20 km^2 surface area, with relatively consistent mineralogy and chemistry. Quartz, alkali feldspars (microcline and perthite), sodic plagioclases and biotite are the main constituents, commonly associated with minor amphibole. Accessory phases include zircon, allanite, apatite, and magnetite.

The country rocks are Upper Carboniferous-Lower Permian sandstones and dolomitic limestones. Scattered patches of skarn-type assemblages dominated by tremolite and talc occur in the dolomitic limestones, and sandstones are recrystallized to a coarse-grained quartzite at contact with the granite. The granite is metaluminous to slightly peraluminous, and is distinguished by high FeO_t/MgO ratios, typical of ferroan (A-type) granites. The A-type affinity is also reflected by high Na_2O+K_2O, high Ga/Al ratios, high contents of large ion lithophile elements (LILE), high field strength elements (HFSE) and rare earth elements (REE), as well as low contents of Sr, and distinct negative Eu anomalies. The biotites are aluminous, Fe-rich, and plot near the siderophyllite corner in the quadrilateral biotite diagram. They are further distinguished by high fluorine contents (0.61 to 1.33 wt %). Amphibole is ferrohastingsite in composition. Ion microprobe analyses of zircon grains

separated from a representative granite sample yielded concordant U-Pb ages with weighted mean $^{206}Pb/^{238}U$ age of 288.3 ± 3.6 Ma.

The granite and the country rocks are cut by a set of mafic dykes with asthenosphere-like geochemical signatures. Such association suggests anorogenic intraplate magmatism in Lower Permian in the region. This provides further evidence for, and significantly constrains timing of, a major extension in Upper Paleozoic in Iran, previously inferred from the rock record. The extension led to the Gondwana break-up and the Opening of Notethys Ocean between Sanandaj-Sirjan and Zagros in Permian.

Keywords: Hasanrobat; Sanandaj-Sirjan belt; A-type granite; Permian; Neotethys; Gondwana

1. Introduction

The Iranian plateau consists of several geological units delineated by major boundary faults, deformation history, and/or suture zones of oceanic character (Fig. 1). Following the Late Precambrian (Katangan) orogeny and the consolidation of the basement, the Precambrian craton of lran became a relatively stable continental platform with shelf deposits dominated by clastic sediments, and lack of major magmatism and deformation during most Paleozoic (e.g. Berberian and King, 1981; Aghanabati, 2009). There is strong stratigraphic and paleomagnetic evidence that from late Precambrian to late Paleozoic times, Iran was a part of Gondwanaland and most likely an extension of the Afro-Arabian continental platform (Stocklin, 1968; Berberian and King, 1981; Ghavidel-Syooki, 1995).

The Sanandaj-Sirjan metamorphic-plutonic Belt (SSB) extends for 1500 km, with an average width of 150 km, in NW-SE direction, parallel to the Zagros fold-thrust system. The SSB

extends northwestward into Turkey, where it is known as Taurus orogenic belt (e.g. Bozkurt et al., 2000; Robertson et al., 2007).

The SSB, Central Iran and Zagros shared a similar history during most of the Paleozoic, all being part of the Gondwana or Afro-Arabian plate (Alavi, 1994). Post-Permian sedimentary rocks in SSB and Central Iran, however, display Eurasian affinities (Stocklin, 1968; Berberian and King, 1981; Davoudzadeh and Weber-Diefenbach, 1987; Hooper et al., 1994). The sedimentary sequences, the main Mesozoic and Cenozoic unconformities, and the structural framework of the SSB are comparable to those of the Central Iran and contrast significantly with the Zagros (Tillman, 1981). However, SSB differs from Central Iran in that the Tertiary sediments are only locally developed, and the dominant northwest trend of the Zagros structures is overprinted on the older structures in the SSB (Tillman, 1981). Berberian and King (1981) argued that SSB-Central Iran began rifting from the Zagros basin by opening of the Neotethys Ocean in Permian. Mohajjel et al. (2003) suggested that rifting and sea-floor spreading occurred in Permian-Triassic times, followed by subduction and demise of the oceanic crust in Upper Jurassic-Cretaceous times.

The SSB is known as a polyphase terrain, experiencing several episodes of deformation, metamorphism and magmatism through time (Tillman, 1981; Mohajjel et al., 2000, 2003; Hassanzadeh et al., 2008). Metamorphic rocks in the SSB include various schists, marbles and metasandstones originating from sedimentary and volcanic protoliths, as well as granitic gneisses. Metamorphic grade ranges from sub-greenschist to amphibolite, with greenschist grade dominating throughout the belt.

Numerous granitoid intrusions occur in the SSB (Fig. 2). The intrusions may occur as discrete bodies, or more commonly, as composite bodies, or complexes, consisting of two or more

intrusions intruding in different pulses at different times. They vary in size from small plutons, <1 km^2 in area, to batholiths, hundreds of square kilometers in extent. Most intrusions are elongated in northwest-southeast direction, parallel to the Zagros main structural trend, and the general trend of foliation and fold axes in the country rocks. They are sheared and mylonitized at various scales. The granitoids are dominated by biotite-granite, biotite-hornblende granodiorite and hornblende-biotite quartz-diorite. Mafic rocks are common, particularly to the north of the SSB, and occur as separate bodies, or more commonly, associated with granitoids in composite bodies.

The granitic intrusions vary in age from Neoproterozoic (Hassanzadeh et al., 2008) to Eocene (Braud, J., 1987; Mahmoudi et al., 2011). However, most intrusions have been indicated to be of Jurassic-Paleocene times (e.g. Berberian and Berberian, 1981; Berberian et al., 1982; Masoudi et al., 2002; Mohajjel et al., 2003; Nezafati et al., 2005; Shahbazi et al., 2010). The intrusions are dominantly calc-alkaline and display features characteristic of I-type granitoids emplaced in a continental arc setting (e.g. Berberian and Berberian, 1981; Ghalamghash, 2001; Masoudi et al., 2002; Alirezaei, 2004; Sepahi and Athari, 2006). The magmatic arc is considered to be related to the subduction of Neotethys oceanic crust underneath Sanandaj-Sirjan belt (Berberian and King, 1981; Berberian and Berberian, 1981; Braud, 1987; Agard et al, 2005; Shahbazi et al., 2010).

We present whole rock geochemistry, mineral chemistry, and geochronology data for Hasanrobat granite in the central SSB, and discuss the implications of the data in the context of the evolution of the SSB. A comparison is also made with the dominant, Jurassic-Paleocene, I-type granitoids to further emphasize the nature and significance of the Hasanrobat granite.

2. Materials and methods

This study is based on the field work, transmitted and reflected light microscopy, as well as whole rock geochemistry, mineral chemistry, and geochronology. Some 16 samples were selected for whole rock analysis, following a detailed petrography of a larger set of samples. The samples were powdered to <200 mesh by agate mill, and the pulps were analyzed by ICP-AES (major oxides) and ICP-MS (minor and trace elements) following a $LiBO_2$ fusion and aqua regia digestion at the ACME laboratories, Vancouver, Canada. The base and precious metals were analyzed by ICP-MS following aqua regia dissolution of pulps. The precision and accuracy, as indicated by duplicates and the USGS standards, are within 1% for major oxides and 10% for minor and trace elements.

The composition of biotite and feldspars from two representative samples was investigated using a Camebax MBX electron microprobe at the Ottawa-Carleton Geosciences Centre, Ottawa, Canada. The operating conditions were 15 kV accelerating voltage, 20 nA beam current and counting times of about 30 seconds or 40000 counts. Raw data were converted to elemental wt% by the Cameca PAP matrix correction program. Analysis is accurate to 1-2% of the quoted values for major elements and 3-5% for minor elements. The composition of amphibole from the same samples was analyzed using a JEOL SuperProbe electron microprobe analyzer at the Department of Earth and Space Sciences at the University of California, Los Angeles (UCLA).

Representative samples from several Jurassic-Paleocene granitoids in the central and northern SSB were analyzed employing the same methods and in the same lab. The data are used for comparison in various discrimination diagrams presented for Hasanrobat granite, and discussed in the text.

Our U-Pb age determination is based on U, Pb, and Th isotopic measurements employing spot analysis on zircon rims using the Cameca IMS 1270 ion microprobe at the University of California, Los Angeles (UCLA). Analytical methods follow the procedures described by Quidelleur et al. (1997) and Schmitt et al. (2003a, 2003b). Following mineral separation using conventional liquid and magnetic techniques, clear euhedral zircon grains were hand selected, mounted in epoxy, and coated with ~100 Å of gold. The ion-microprobe spot analyses utilized a primary ion beam focused to an ~30 μm diameter spot and a secondary ion beam with a mass resolving power of 5,000 and energy window of 50 eV. Following a pre-sputtering period of ~180 seconds, each analysis collected data for 8–10 cycles. The sample chamber was flooded with oxygen at ~3 × 10–5 Torr to enhance secondary Pb ionization. The reported weighted- mean ages are based on $^{206}Pb/^{238}U$ ages calculated using zircon standard AS3 (1099 ± 0.5 Ma; Paces and Miller 1993). Common lead corrections were made using the measured values of ^{204}Pb (Stacey and Kramers, 1975) and the values of ^{208}Pb corrected for ^{232}Th-derived ^{208}Pb (Compston et al., 1984), which are considered a proxy for common ^{206}Pb and ^{207}Pb. These corrections use the anthropogenic Pb compositions reported for the Los Angeles basin (Sanudo-Wilhelmy and Flegal, 1994). All age uncertainties are reported at the 1σ level.

3. Geology background

The Hasanrobat pluton lies in the Mooteh-Laybid area in the Golpaygan quadrangle, Central SSB (Fig. 2). The quadrangle has been the focus of many studies due to its varied geology as well as the occurrence of gold deposits, represented by Mooteh (Moritz et al., 2006), Pb-Zn deposits, and dimension stones. It is noteworthy that Golpaygan quadrangle was the first

geological map at 1/250,000 scale prepared by Geological Survey of Iran (Thiele et al., 1968).

The Golpaygan quadrangle is characterized by extensive outcrops of Precambrian metamorphic rocks, represented by metasandstones and various schists. The metamorphic rocks are overlain successively by Infracambrian Kahar slates and Soltanieh dolomites, the Cambrian Zaigun shales and Lalun sandstones, and the Upper Cambrian-Lower Ordovician Mila limestones and dolomites (Thiele et al., 1968).

The Ordovician-Carboniferous sediments are variably missing in the rock record from SSB and most other parts of Iran, a feature attributed to epeirogenic movements associated with the Caledonian and Hercynian orogenies in Europe and northwest Africa (Stocklin, 1968; Berberian and King, 1981; Aghanabati, 2009). In the Golpaygan quadrangle, the Permian strata overlie disconformably the Cambrian and Ordovician sediments (Thiele et al., 1968; Aghanabati, 2009). The Upper Carboniferous-Lower Permian transgression, documented from various localities in Iran, is represented by a basal sandstone grading upward into a thick carbonate sequence (Aghanabati, 2009; Alavi-naini, 2009).

Four major episodes of deformation are recorded in the Central SSB during Mesozoic-Cenozoic, consistent with various stages of opening, subduction, and closure of the Neotethys Ocean, and subsequent continental collision (e.g. Tilmann et al., 1980; Mohajjel et al., 2003). The main phase, leading to extensive deformation, metamorphism, and magmatism, occurred in Upper Cretaceous-Paleocene times. The ophiolite sequences at SSB-Zagros boundary represent remnants of the Neotethys oceanic lithosphere (Berberian et al., 1982; Mohajjel et al., 2003).

The main structural features, such as folds' axes and axial planes, dominantly strike in northwest-southeast direction. The thrusts are mainly directed southwest, and northwest-trending reverse faults led to the thickening of the crust and subsequent uplift in Tertiary (Mohajjel et al., 2003; Agard et al., 2005). Tilmann (1981) showed that the central SSB consists of several structural blocks separated by regional northwest trending fault zones, and that folding, metamorphism, and thickening of crust were associated mostly with large scale reverse and translational movements along the four major fault zones.

The occurrence of granitic intrusions in the Golpaygan quadrangle was first reported by Thiele (1968) who divided the intrusions into three groups based on cross-cutting relations, and by analogy with other plutons in SSB. A Precambrian age was proposed for the oldest group, represented by Hasanrobat, Mooteh and Cheshmeh-Sefid (Fig. 2). The second group, thought to be of Upper Jurassic-Lower Cretaceous times, includes intrusions in north and east Aligoodarz and south Golpaygan. The third group includes small intrusions in north-northwest Golpaygan that clearly cut through the Cretaceous strata and are considered to be of Tertiary age (Fig. 2).

An intrusive complex, dominated by coarse-grained, light colored granite, occurs in the Mooteh area, ~20 km northwest of the Hasanrobat pluton (Fig 2). Hassanzadeh et al. (2008) reported zircon U-Pb ages of 578 ± 22 Ma and 588 ± 23 for the dominant leucogranite in the Mooteh area. The authors reported a similar crystallization age (zircon U-Pb: 588±23 Ma) for a granitic gneiss in Hajqara Mountains, Varzaneh (Fig. 2), ~25 km to the west of the Mooteh granite

The peak thermal metamorphism in the Mooteh-Laybid area is constrained by a K-Ar age of 174.5 ± 2.9 Ma for an amphibolite (Rachidnejad-Omran et al., 2002). The K-Ar ages of

68±1.0 Ma and 60±0.9 Ma earlier reported for the Mooteh granite and the Hajqara granitic gneiss, respectively (Rachidnejad-Omran et al., 2002) and the Ar-Ar age of 72±2 Ma reported for the Mooteh granite (Moritz et al., 2006) seem to be representing a major thermal event in the area, consistent with the main phase of deformation in the central SSB.

The Cheshmeh-Sefid pluton, 10 km north Golpaygan (Fig. 2) is a composite body consisting of quartz-monzonite to quartz-syenite, granite and syenite (Davoudian et al., 2007). The authors interpreted the pluton as an A-type granitoid emplaced at deep levels (17-20 km) in the crust. Considering the small number of samples analyzed, and the large discrepancy in the data, such interpretation would be unrealistic. Compared to Hasanrobat, and other A-type granites reported in the literature, the Cheshmeh-Sefid pluton is not much enriched in REEs, HFSEs and LILEs and cannot be classified as an A-type granite.

3-1. Country rocks around Hasanrobat pluton

The country rocks surrounding Hasanrobat granite include Upper Paleozoic sandstones and dolomitic limestones, and Triassic-Jurassic shales and sandstones, metamorphosed under sub-greenschist to greenschist grades. (Figs. 3 and 4A). The Paleozoic strata are considered as equivalents of the Dorud and Ruteh Formations (Moosavi, 2003) where Upper Carboniferous-Lower Permian, and Lower Permian ages, respectively, have been proposed for the non-metamorphosed equivalents elsewhere in Alborz and Central Iran (Aghanabati, 2009; Alavi-naini, 2009). The Triassic- Jurassic strata are considered as equivalents of Nayband and Shemshak Formations in Central Iran and Alborz (Moosavi, 2003). Thiele (1964) reported the occurrence of basaltic lavas in the Permian strata in the Golpaygan quadrangle.

To the north, west, and east, the country rocks are covered by Quaternary alluvium. To the south, however, the rocks are well exposed, and field relations can be conveniently investigated. The sandstones recrystallized to coarse-grained quartzite (Fig. 4B) and calc-silicate assemblages, dominated by tremolite and talc, developed in the dolomitic limestones (Fig. 4-C). The skarn type rocks are creamy to brownish in color and occur in small, scattered patches and lenses, up to 4 meters thick, near the granite contact. The field relations, in particular the contact metamorphic aureole, indicate that the Hasanrobat pluton is in intrusive contact with the Upper Carboniferous-Lower Permian sandstones and dolomitic limestones. This argues against a recent study by Mansouri Esfahani et al. (2010) who considered the contacts between the granite and the country rocks as faulted and assumed a Precambrian age for the granite, following Thiele et al. (1968).

3-2. Granite

The Hasanrobat granite occurs as an oval-shaped body, ~20 km^2 surface area, intruding into the Upper Carboniferous-Lower Permian strata (Figs. 3 and 4A-B). The granite is medium- to coarse-grained, and grayish to pinkish in color. Textures vary from dominantly granular in the inner parts to increasingly porphyroid towards the margins, the latter characterized by the occurrence of coarse to very coarse feldspars (10-20 mm in diameter) in a medium-grained matrix. The contrasting rheology of granite and the country rocks during deformation led to intense shearing of the granite towards the margins. The granite was granulated and mylonitized, leading to the development of a gneissic texture, particularly near the contacts with the Permian sandstones and carbonates.

The Hasanrobat pluton displays a rather consistent mineralogy. Quartz, K-spar (mainly microcline), biotite and plagioclase are the main constituents (Fig. 4D), commonly associated

with minor amphibole. Subsolidus exsolution texture, represented by perthite, is common, and equilibrium quartz-feldspar intergrowth textures (i.e., myrmeckitic and graphic textures), are locally developed. The pluton is essentially subsolvus in nature; however, minor occurrence of hypersolvus granite with ferrohornblende and acmite in the norm has been reported by Mansouri Esfahani et al. (2010).

Microcline and perthite occur as discrete grains, <10 mm in diameter, interstitial to quartz and plagioclase, as well as very coarse grains poikilitically enclosing the latter minerals. Biotite occurs as discrete subhedral to anhedral grains, as well as grain aggregates interstitial to feldspars and quartz. Amphibole occurs as bluish green, subhedral grains commonly associated with biotite, and partially replaced by this mineral. Textural relations suggest that the two minerals appeared late in the crystallization history of the granite.

Accessory phases include zircon, allanite, apatite, titanite, and magnetite. Zircon is abundant and was among the first minerals to start to crystallize from the melt. It is common as fine (<1 mm) euhedral inclusions in plagioclase (Fig. 4E), but absent or rare in K-spars, implying that the parent magma was saturated with zircon at high temperatures. Apatite displays a rather similar behavior to zircon. Allanite occurs as brownish, euhedral to subhedral crystals interstitial to the major minerals.

Minor muscovite and chlorite locally occur as post-solidus, alteration products replacing earlier magmatic minerals, particularly biotite. Titanite occurs both as a primary magmatic phase as well as a post-solidus alteration product replacing biotite. Magmatic titanite occurs as euhedral to subhedral grains, interstitial to, or enclosed by, other silicates, whereas the alteration titanite occurs commonly as anhedral grains and grain aggregates. A more detailed description of the granite is presented in Mansouri Esfahani et al. (2010).

Aplitic dykes are common, particularly towards the margins of the pluton. The dykes consist mainly of quartz (>80%), microcline (<10%), sodic plagioclases (<10%) and biotite (<5%). Accessory phases include titanite and zircon. The dykes vary in length and width between 5-100m and 2-100 cm, respectively. Small pods of quartz-feldspar pegmatites locally occur in the granite.

Features commonly considered as evidence for shallow emplacement, i.e. compositional zoning in plagioclases, occurrence of quartz as embayed bipyramidal crystals, abundant aplites, miarolitic cavities and podiform pegmatites, and quartz-feldspars graphic intergrowths (e.g. Burnham and Ohmoto, 1980; King et al., 1997) and reported from many A-type granites worldwide (e.g. King et al., 1997; Charoy and Raimbault, 1994) are uncommon in the Hasanrobat granite, and in this respect, the granite appears to be a rather deep-seated intrusion.

3-3. Biotite-rich enclaves

The granite contains enclaves of dark, biotite-rich materials, particularly towards the margins. The enclaves are mostly sub-rounded in shape, and vary in size commonly from few centimeters to 50 cm. They are medium- grained and dominantly equigranular in texture, and display the same mineral assemblage as the enclosing granite; however, they are distinguished by more abundant biotite, and less quartz. As in the granite, the enclaves contain abundant fine zircons.

3-4 Mafic dykes

Mafic dykes locally occur in the granite, as well as in the Carboniferous-Permian dolomitic limestones. The dykes vary in length and thickness between 50-500 m and 2-5 m, respectively. They display the same deformation as in their host rocks, implying that they

predate the main regional deformation in the area. This is best displayed in a quarry in the Laybid area, some 10 km west of the Hasanrobat pluton, where the mafic dykes in the dolomitic limestones are boudined and deformed (Fig. 4F).

The mafic dykes are subophitic in texture and consist of plagioclase laths, amphiboles (tremolite-actinolite) and lesser biotite, chlorite, and epidote. Titanite, apatite and Fe-Ti oxides are common accessory phases. Relics of clinopyroxenes are common. The mineral assemblage suggests that the mafic dykes experienced retrograde reactions and re-equilibrated under the ambient P-T conditions after emplacement. This was associated with the replacement of the original pyroxene and olivine? by tremolite-actinolite and chlorite. The Hasanrobat mafic dykes probably belong to the same magmatic phase that generated the basaltic lavas in the Permian strata throughout the region (e.g. Thiele et al., 1968).

4. Geochemistry

The chemical analyses of the Hasanrobat pluton, the dark biotite-rich enclaves, and the mafic dykes are listed in Table 1. The pluton displays a rather consistent chemistry, with the SiO2 contents in the range 68-74 wt%. On $Q'(F')$-ANOR diagram (Streckeisen and Le Maitre, 1979), most samples plot in the syenogranite domain. The granite is metaluminous to slightly peraluminous, and is distinguished by high FeO_t/MgO ratio, in the range 8-14. On the SiO_2 vs FeO/(FeO+MgO) discrimination diagram (Frost et al., 2001), the Hasanrobat pluton plots in the ferroan (A-type) domain, while the SSB dominant Jurassic-Paleocene granitoids plot in the magnesian, Cordilleran domain (Fig. 5A). The pluton further plots in the alkali-calcic domain in the modified alkali lime index (Na2O + K2O - CaO) vs SiO2 discrimination diagram of Frost and Frost, 2011 (Fig. 5B).

The Zr contents vary between 265-454 ppm yielding zircon saturation temperatures (Watson and Harrison, 1983) between 825 and 870 ^{o}C. This is consistent with data from mineralogically similar A-type granites in the Lachlan fold belt, Australia (King et al., 1997) and the Amazonian craton (Dall'Agnoll et al., 1999).

The Hasanrobat granite displays steep REE patterns with strong enrichments in LREE relative to HREE and distinct negative Eu anomalies (Fig. 6). The La_N/Yb_N ratio varies between 5.8-9.4. A similar pattern, but lacking Eu anomaly, is shown by the mafic dykes, with the La_N/Yb_N ratio in the range 4.7-7.2. The biotite-rich enclaves are less fractionated. They are relatively depleted in LREE and enriched in MREE and HREE. The Hasanrobat granite is distinguished from the SSB Jurassic-Paleocene, dominantly I-type granitoids by considerably higher contents of REE. However, no significant differences in the REE patterns, or slopes, can be established between the two types of granites.

The Hasanrobat granite is also distinguished by strong enrichments in LILE and HFSE (Fig. 7), features commonly known as characteristic of A-type granites (e.g. Collins et al., 1982; King et al., 1997; Dall'Agnoll et al., 1999; Lenharo et al., 2002). A similar pattern is displayed by the biotite-rich enclaves; however, the enclaves are relatively enriched in the compatible elements, Sr, P, and HREE, and depleted in most incompatible elements, including LREE, Ba, U, and Th. This difference in the minor and trace element chemistry is also reflected in the major elements, where the enclaves are considerably enriched in the compatible elements, Mg, Ca, and Ti, and depleted in Si.

On the Rb vs Yb+Nb discrimination diagram (Pearce et al, 1984), the Hasanrobat granite and the enclaves plot in the "within plate" domain, while the SSB Jurassic-Paleocene granitoids fall in the "volcanic arc" domain (Fig. 8A). The A-type affinity of the granite is further

emphasized by plots of the granite in the Zr vs 10000*Ga/Al and FeOt/MgO vs Zr+Nb+Ce+Y discrimination diagrams of Whalen et al. (1987), where a clear distinction exists between the Hasanrobat granite and the SSB Jurassic-Paleocene I-type granitoids (Figs. 8B-C).

A-type granites are important sources of W, Sn, Ta, Nb, Zr, Hf, Be, U, F, and REE (e.g. Collins et al., 1982; Heinhorst et al, 2000; Lenharo et al., 2002). The Hasanrobat granite is enriched in Sn and W, by a factor of ~4, compared to the Jurassic-Paleocene I-type granitoids. Similarly, the granite is enriched in high field strength elements and rare earth elements (Fig. 8). However, no mineralization is associated with the granite at the current exposures. This could be due to deep erosion of the granite. Alternatively, this might be attributed to the deep emplacement of the granite, as its texture suggests, preventing retrograde boiling and exsolution of a hydrothermal fluid from the magma.

5. Mineral chemistry

The compositions of selected biotites, amphiboles, and feldspars are shown in Table 2. The biotites are aluminous, Fe-rich, and plot near the siderophyllite corner in the biotite quadrilateral diagram (Fig. 9). The biotites are also distinguished by elevated concentrations of fluorine (0.61 to 1.33 wt% F). Biotites of similar composition have been reported from many A-type granites worldwide (e.g. Neymark et al., 1996; Colombo et al., 2000; Lenharo et al., 2002). The amphiboles are ferrohastingsite in composition (c.f. Stull, 1973), and compare in chemistry with the amphiboles reported from several A-type granites in the Lachlan Fold Belt, Australia (King et al., 1997). The plagioclases are considerably rich in the albite component (Table 2).

6. Geochronology

Following the detailed petrography, sample 05HSR, a pinkish gray, coarse-grained biotite granite, representing the dominant rock in the Hasanrobat granite, was selected for zircon U-Pb geochronology. Zircons in the Hasanrobat granite are mostly euhedral and show elongation ratios between 2 and 2.5 suggesting a primary magmatic origin (Mansouri Esfahani et al., 2006). Rims of ten handpicked clear euhedral whole grains from this specimen were individually analyzed with ion microprobe, from which nine yielded concordant U-Pb ages with weighted mean $^{206}Pb/^{238}U$ age of 288.3 ± 3.6 Ma and MSWD = 0.86 (Appendix 1). Figure 10 is a Tera-Wasserburg presentation of concordant ages of these zircons by using ISOPLOT (Ludwig, 2003).

7. Discussion and Conclusions

The Hasanrobat pluton occurs as an isolated body intruding into the Upper Carboniferous-Lower Permian strata. The pluton is dominantly syenogranite in composition and consists of quartz, microcline, sodic plagioclase, biotite and minor ferrohastingsite. The granite lacks olivine or pyroxene and in this regard resembles the aluminous A-type granites of Lachlan fold belt, Australia (King et al., 1997) and the Jamon granite in the Amazonian craton (Dall'Agnoll et al., 1999).

The granite is metaluminous to slightly peraluminous, and is distinguished by high Na_2O+K_2O, high $Fe_{(total)}/Fe_{(total)}+Mg$ and Ga/Al ratios, high abundances of LILE, HFSE and REE, and low abundances of Fe–Mg trace elements (Cr, V, Ni, Cu), Ba, Sr and Eu, features commonly known as characteristic of A-type granites, as first introduced by Loiselle & Wones (1979) and later by various authors (e.g. Collins et al., 1982; Whalen et al., 1987; King et al., 1997; Dall'Agnoll et al., 1999; Rämö et al., 2002). The Hasanrobat granite further

corresponds to the A-type granites of the aluminous (King et al., 1997) and A-1 (Eby, 1992) subtypes.

The occurrence of magnetite, and not ilmenite, as accessory phase, in the Hasanrobat granite suggests that the granite crystallized from a relatively oxidized magma. This also explains the occurrence of titanite as a primary magmatic phase in the granite. The oxidized nature of the granite is also implicated in the relatively high Fe^{+3}/Fe^{+2} ratios in the whole rock analyses reported in Mansouri Esfahani et al. (2010). A-type granites are commonly known to be reduced, fO_2 < Q-F-M quartz-fayalite-magnetite (e.g. Emslie and Sterling, 1993; Frost and Frost, 1997; Frost et al., 1999); however, relatively oxidized, magnetite- and titanite bearing examples have been reported from several localities, including Amazonian craton (Dall'Agnoll et al., 1999; Rämö et al., 2002), and southwestern United States of America (Anderson and Bender, 1989).

No significant mafic or intermediate fractions can be distinguished associated with the granite. This argues against derivation from intermediate magmas, but considerable fractionation of silicic magma, as variations in chemistry in the pluton suggests, is not precluded. The A-type chemistry of the Hasanrobat granite appears to be a feature mainly controlled by the conditions of melting in the source region. The largely metaluminous composition of the Hasanrobat granite, indicated by relatively low molar Al2O3/CaO+Na2O+K2O values, and the homogeneous zircon grains suggest that the parent magma originated from a homogenous source and that metasedimentary crustal components did not much influence the magma composition.

The abundant dark, biotite-rich enclaves in the Hasanrobat granite display the same A-type features as their enclosing granite. The enclaves are distinguished by higher contents of the

major elements Fe, Mg, Ca, Ti, P, Mn, as well as those trace elements (e.g. Ni, Cr, V, Co, and HREE) that are commonly known to be compatible during crystallization of felsic-intermediate magmas. Variations in chemistry in the two rocks can best be explained by fractional crystallization processes. We interpret the enclaves as fragments of the previously solidified materials from the roof and the walls, engulfed by the residual granitic magma. The slightly higher contents of the incompatible, highly mobile elements, Cs, Rb, U, and Th in the enclaves can be attributed to reequilibration with the enclosing magma.

Many A-type granites are associated with extrusive equivalents, typical examples being the Lachlan Fold Belt, Australia (King et al., 1997) and the northern Kordofan, central Sudan (Vail, 1985). No extrusive equivalents, or plutons with similar chemistry, have yet been reported from the area around Hasanrobat. This is an issue to be investigated in the future.

The Hasanrobat granite and the Upper Carboniferous-Lower Permian country rocks are associated with a set of mafic dykes. The granite and the mafic dykes are both characterized by element ratios similar to those observed for asthenospheric rocks (Figs. 11A-B), implying a genetic relation between the two rock types. The mafic dykes show trace element patterns similar to those of E-MORB indicating an asthenospheric source. Association of A-type granite and E-MORB type mafic dikes at Hasanrobat resembles the well-known examples of coeval mafic and silicic magmas with such chemical affinities (e.g. Kűster, 1993; Heinhors et al, 2000; Rämö and Frindt, 2005; Katzira et al., 2007) and suggest anorogenic intraplate magmatism in Lower Permian in the region.

After a long period of epeirogeny and significant hiatuses in the sedimentary record during Ordovician-Carboniferous, Upper Carboniferous-Lower Permian was a time of marine transgression associated with a major extensional phase that affected most parts of Iran

(Berberian and King, 1981; Alavi-naini, 2009). This phase was mainly developed along the Sanandaj-Sirjan belt, represented by basic volcanic rocks (Thiele et al., 1968; Berberian and King, 1981; Aghanabati, 2009).

The A-type Hasanrobat granite with the new zircon U-Pb age of 288.3 ± 3.6 Ma temporally correlates with the Lower Permian syn-rift volcanics along the Tethyan orogenic belt (e.g., Garzanti et al., 1999; Chauvet et al., 2008) and records the Gondwana break-up in Iran. This age significantly constrains timing of the break-up and the Neotethys Ocean opening between Sanandaj-Sirjan and Zagros-Arabia which was inferred to be Permian based on the sedimentary record (e.g. Berberian and King, 1981; Aghanabati, 2009). Through this rifting event, underplating by asthenospheric mafic magmas led to the fusion of lower crust to produce the parent granitic melt of the Hasanrobat pluton; the same way it has been articulated for generation of the A-type granites north of the Red Sea (Coleman et al., 1992) and elsewhere (e.g. Lachlan Fold Belt, Australia, King et al., 1997; Rio Maria region, Eastern Amazonian craton, Brazil, Rämö et al., 2002; Telemark, southern Norway, Andersen et al., 2007). The alkali-calcic nature of the Hasanrobat granite favors low-pressure partial melting of a tonalitic to granodioritic crust (c.f. Frost and Frost, 2011). The occurrence of homogeneous zircon grains in the granite argues against significant contamination by metasedimentary crustal components.

The Middle-Upper Triassic andesitic-basaltic volcanism and associated intrusive rocks in the Eqlid area in southern SSB, and the dominantly I-type Jurassic-Paleocene granitoids in the central and northern SSB are considered to be associated with the subduction of Neotethys oceanic crust underneath Sanandaj-Sirjan belt (Berberian and King, 1981; Berberian and Berberian, 1981; Braud, 1987; Agard et al, 2005; this study).

Acknowledgements

This study was partly supported by the Shahid Beheshti University grant No. 600/3205 to SA. The U-Pb data acquisition at UCLA has benefited from valuable assistance by Axel Schmitt and the National Science Foundation grant EAR-0337775 to Horton and Axen. The ion microprobe facility at UCLA is partly supported by a grant from the Instrumentation and Facilities Program, Division of Earth Sciences, National Science Foundation.

Figure Caption

Figure 1. The main geological divisions (provinces) of Iran (simplified after Stocklin and Setudenia, 1970; Berberian and King, 1981). The rectangle shows the outlines of the geological map shown in Figure 2.

Zagros: Phanerozoic continental shelf sediments deposited in a passive margin setting; Sanandaj-Sirjan: Late Precambrian-Mesozoic metamorphosed sedimentary-volcanic rocks, and granitoid intrusions; Central Iran: Late Precambrian-Mesozoic continental shelf deposits overlying a Precambrian crystalline basement, and Cenozoic volcanic-plutonic rocks distributed mainly in the west, east and north. Zabol-Baluch and Makran: Post-Cretaceous flysch-molasse deposits overlying Cretaceous ophiolite mélange. Alborz: Paleozoic-Mesozoic sediments covered by Cenozoic volcanic and sedimentary materials; Kopet Dagh: Mesozoic-Cenozoic shallow marine sediments;

Figure 2. Geological map of the central Sanandaj-Sirjan belt (simplified after NIOC, 1975). The square shows the location of the Golpaygan quadrangle, discussed in the text.

Figure 3. Geological map of the Hasanrobat area (modified after Moosavi, 2003).

Figure 4. (A) A general view of the Hasanrobat granite (brownish, left), the Upper Paleozoic sandstones and dolomitic limestones (creamy, middle) and Triassic-Jurassic sandstones and

shales (dark grey, right). The width of the view is about 5 km. (B) An outcrop showing the Upper Paleozoic sandstones (reddish, upper part) at contact with the granite (creamy, lower part). The reddish color of the sandstone is due to iron-oxide staining. (C) Photomicrograph of the tremolite-talc skarn showing elongated tremolite crystals (yellowish to reddish crystals) embedded in calcite; XPL. (D) Photomicrograph of the Hasanrobat granite, displaying the main constituents, microcline, plagioclase, quartz and biotite; XPL. (E) Photomicrograph showing the occurrence of zircon crystals in plagioclase, a common feature in the Hasanrobat granite; XPL. (F) A mafic dyke, boudined and deformed, in the Upper Paleozoic dolomitic limestones; photo from a quarry in Laybid, ~10 km west of the Hasanrobat granite.

Figure 5. (A) Plots of the Hasanrobat granite and the biotite-rich enclaves in the SiO_2 vs FeOt/FeO+MgO discrimination diagram (Frost et al., 2001), showing a ferroan affinity for the rocks. Domain for the Sanandaj-Sirjan belt Jurassic-Paleocene granitoids is shown for comparison. (B) Plots of the Hasanrobat granite and the biotite-rich enclaves in the modified alkali lime index (Na2O + K2O - CaO) vs SiO_2 discrimination diagram of Frost and Frost (2011) showing an alkali-calcic nature for the rocks.

Figure 6. Chondrite-normalized rare earth element (REE) patterns for the Hasanrobat granite (hatched), the biotite-rich enclaves (circles) and the mafic dykes (diamonds). Variations for the Sanandaj-Sirjan belt Jurassic-Paleocene granitoids (shaded) are shown for comparison. The Mafic dykes show clear E-MORB affinity. Normalizing values after Sun and McDonough (1989).

Figure 7. Primitive mantle-normalized multielement patterns for the Hasanrobat granite (hatched), the biotite-rich enclaves (circles), and the mafic dykes (diamonds). Variations for

the Sanandaj-Sirjan belt Jurassic-Paleocene granitoids (shaded) are shown for comparison. Normalizing values after Sun and McDonough (1989).

Figure 8. Plots of the Hasanrobat granite (open squares) and the biotite-rich enclaves (solid squares) on (A) the Rb vs Yb+Nb discrimination diagram of Pearce et al. (1984), (B) the Zr vs 10000*Ga/Al discrimination diagram of Whalen et al. (1987) and (C) the FeOt/MgO vs Zr+Nb+Ce+Y (ppm) discrimination diagram of Whalen et al. (1987), showing a within-plate setting and A-type affinity for the granite and the enclaves. Domains for the Sanandaj-Sirjan belt Jurassic-Paleocene granitoids (gray field) are shown for comparison.

VAG: volcanic arc granite; WPG: within plate granite; Syn-COLG: syncollision granite; ORG: ocean ridge granite.

Figure 9. Plots of the Hasanrobat biotite analyses on the biotite quadrilateral diagram, showing a dominantly siderophyllite composition.

Figure 10. Concordia diagram showing ion microprobe zircon U-Pb data for the Hasanrobat granite.

Figure 11. Plots of the Hasanrobat granite and the mafic dykes on the Yb/Ta vs Y/Nb (A) and Ce/Nb vs Y/Nb (B) discrimination diagrams of Eby (1992), showing an OIB affinity for the rocks.

References

Agard, P., Omrani, J., Jolivet, L., Mouthereau, F., 2005. Convergence history across Zagros (Iran): Constraints from collisional and earlier deformation: International Journal of Earth Sciences, 94, 401-419.

Aghanabati, A., 2009. Stratigraphic Lexicon of Iran, V. 2. Devonian-Permian. National Geosciences Directory of Iran, Geological Survey of Iran.

Alavi, M., 1994. Tectonics of the Zagros orogenic belt of Iran: New data and interpretations: Tectonophysics, 229, 211–238.

Alavi-naini, M. (2009) Stratigraphy of Iran. National Geosciences Directory of Iran, Geological Survey of Iran, 507 p.

Alirezaei, S., 2004. The geochemistry of plutonic rocks from Sanandaj-Sirjan metamorphic-plutonic belt, western Iran. Geological Association of Canada-Mineralogical Association of Canada, Montreal, Canada.

Anderson, J.L., Bender, E.E., 1989. Nature and origin of Proterozoic A-type granitic magmatism in the southwestern United States of America, Lithos 23, 19-52.

Andersen, T., Griffin, W.L., Sylvester, A.G., 2007. Sveconorwegian crustal underplating in southwestern Fennoscandia: LAM-ICPMS U–Pb and Lu–Hf isotope evidence from granites and gneisses in Telemark, southern Norway. Lithos, 93, 273–287.

Berberian, F., Berberian, M., 1981. Tectono-plutonic episodes in Iran: American Geophysical Union, Geodynamic Series, 3, 5–32.

Berberian, F., Muir, I.D., Pankhurst, R.J., Berberian, M., 1982. Late Cretaceous and early Miocene Andean-type plutonic activity in northern Makran and Central Iran. Journal of the Geological Society of London, 139, 605–614.

Berberian, M., King, G.C.P., 1981. Towards a paleogeography and tectonic evolution of Iran: Canadian Journal of Earth Sciences, 18, 210–265.

Bozkurt, E., Winchester, J.G.A., Piper, J.D.A. (eds), 2000. Tectonics and magmatism in Turkey and the surrounding area. Geological Society, London, Special Publication, 173.

Braud, J., 1987, La suture du Zagros au niveau de Kermanshah (Kurdistan iranien): Reconstitution palégéographique, évolution géodynamique, magmatique et structurale: Unpublished Ph.D. thesis, Université de Paris-Sud, 489 p.

Burnham, C.W., Ohmoto H., 1980. Late-stage processes of felsic magmatism. Mining Geology, Special Issue 8, 1-11.

Charoy, B., Raimbault, L., 1994. Zr-, Th-, and REE-rich biotite differentiates in the A-type granite pluton of Suzhou (Eastern China): the key role of fluorine. J. Petrology, 35(4): 919-962.

Chauvet et al., 2008. Geochemistry of the Panjal Traps basalts (NW Himalaya): records of the Pangea Permian break-up. Bulletin de la Societe Geologique de France, 179 (4), 383-395.

Coleman, R.G., DeBari, S., Peterman, Z., 1992. A-type granite and the Red Sea opening. Tectonophysics, 204, 27-40.

Collins, W.J., Beams, S.D., White, A.J.R., Chappell, B.W., 1982. Nature and origin of A-type granites with particular reference to southeastern Australia. Contrib. Mineral. Petrol., 80, 189–200.

Colombo, F., Lirai, R.J., Dorais, M.J., 2010. Mineralogy and crystal chemistry of micas from the A-type El Portezuelo Granite and related pegmatites, Catamarca (NW Argentina). Journal of Geosciences, 55, 43–56.

Compston, W., Williams, I.S., and Meyer, C., 1984. U-Pb geochronology of zircons from lunar breccia 73217 using a sensitive high mass-resolution ion microprobe. Journal of Geophysical Research, 89, B525–B534.

Dall'Agnoll, R., Scaillet, B., Pichavant M., 1999. An experimental study of a lower Proterozoic A-type granite from the Eastern Amazonian craton, Brazil. Journal of Petrology, 40, 1673-1698.

Dall'Agnoll, R., de Oliveira, C.D., 2007. Oxidized, magnetite-series, rapakivi-type granites of Carajás, Brazil: Implications for classification and petrogenesis of A-type granites. Lithos, 93, 3-4, 215-233.

Davoudian, A., Hamedani, A., Shabanian, N., Mackizadeh, M.A., 2007. Petrological and geochemical constraints on the evolution of the Cheshmeh-Sefid granitoid complex of Golpaygan in the Sanandaj-Sirjan zone, Iran. N. Jb. Miner. Abh. 184/2, 117–129.

Davoudzadeh, M., Weber-Diefenbach, K., 1987. Contribution to the paleogeography, stratigraphy and tectonics of the Upper Paleozoic of Iran: N. Jb. Geol. und Pal. Abh, 175, 121–146.

Eby, G.N., 1992. Chemical subdivision of the A-type granitoids: Petrogenetic and tectonic implications. Geology, 20, 7, 641-644.

Emslie, R.F., Stirling, J.A. (1993) Rapakivi and related granitoids of the Nain plutonic suite: geochemistry, mineral assemblages and fluid equilibria. Canadian Mineralogist 31, 821-847.

Frost, B.R., Barnes, C.G., Collins, W.J., Arculus, R.J., Ellis, D.J., Frost, C.D., 2001. A geochemical classification for granitic rocks. J. Petrology, 41, 11, 2033-2048.

Frost, C.D., Frost, B.R., 1997. Reduced rapakivi-type granites: the tholeiitic connection. Geology, 25, 647-650.

Frost, C.D., Frost B.R., Chamberlain K.R., Edwards, B.R., 1999. Petrogenesis of 1.43 Ga Sherman batholith, SE Wyoming, USA, a reduced rapakivi type anorogenic granite. Journal of Petrology, 40, 12, 1771-1802.

Frost, C.D., Frost B.R., 2011. On Ferroan (A-type) Granitoids: their compositional variability and modes of origin. Journal of Petrology, 52, 1, 39-53.

Garzanti, E., Le Fort, P. and Sciunnach, D., 1999. First report of Lower Permian basalts in South Tibet: tholeiitic magmatism during break-up and incipient opening of Neotethys. J. Asian Earth Sci. 17, 533-546.

Ghavidel-Syooki, M., 1995. Palinostratigraphy and paleogeography of a Paleozoic sequence in the Hasankdar area, central Alborz range, northern Iran. Review of Paleobotany and Palinology, 86, 91-109.

Hassanzadeh, J., Stockli, D.F., Horton, B.K., Axen, G.J., Stockli, L.D., Grove, M., Schmitt, A.K., Walker, J.D., 2008. U-Pb zircon geochronology of late Neoproterozoic–Early Cambrian granitoids in Iran: Implications for paleogeography, magmatism, and exhumation history of Iranian basement. Tectonophysics, 451, 1-4, 71-96.

Heinhorst, J., Lehmann, B., Ermolov, P., Serykh, V., Zhurutin, S., 2000. Paleozoic crustal growth and metallogeny of Central Asia: evidence from magmatic-hydrothermal ore systems of Central Kazakhstan. Tectonophysics, 328, 69-87.

Hooper, R.J., Baron, I., Hatcher Jr., R.D., Agah, S., 1994. The development of the southern Tethyan margin in Iran after the break-up of Gondwana - implications for the Zagros hydrocarbon province: Geosciences Iran, v. 4, p. 72–85.

Katzira, Y., Litvinovskya, B.A., Jahnb, B.M., Eyala, M., Zanvilevicha, A.N., Valley, J.W., Vapnika, Y., Beeria, Y., Spicuzzac, M.J., 2007. Interrelations between coeval mafic and A-type silicic magmas from composite dykes in a bimodal suite of southern Israel, northernmost Arabian–Nubian Shield: Geochemical and isotope constraints. Lithos, 97, 336-364.

King, P.L., White, A.J.R., Chappell B.W., Allen, C.M., 1997. Characterization and Origin of Aluminous A-type Granites from the Lachlan Fold Belt, Southeastern Australia. Journal Of Petrology, 38, 3, 371–391.

Kűster, D., Harms, U., 1998. Post-collisional potassic granitoids from the southern and northwestern parts of the Late Neoproterozoic East African Orogen: a review. Lithos, 45,177–195.

Kűster, D., 1993. Geochemistry and petrogenesis of Permo-Jurassic oversaturated alkaline complexes of northern Kordofan, central Sudan. In: Thorweihe, U., Schandelmeier, H. (Eds). Geoscientific Research in NE Africa, Rotterdam, 197–201.

Ludwig, K.R., 2003. Isoplot 3.0. A Geochronological Toolkit for Microsoft Excel, Berkeley Geochronology Center Special Publication No. 4, 70 p.

Lenharo, S.L.R., Moura, M.A., Botelho, N.F., 2002. Petrogenetic and mineralization processes in Paleo- to Mesoproterozoic rapakivi granites: examples from Pitinga and Goia´s, Brazil. Precambrian Research, 119, 277-/299.

Mansouri Esfahni, M., Kochhar, N., and Gupta, L.N., 2006. Morphological studies of zircons from the Hasanrobat granite and associated rocks, Esfahan, Iran. Ind. Min. 40, 49-58.

Mansouri Esfahani, M., Khalili, M., Kochhar, N., Gupta, L.N., 2010. A-type granite of the Hasanrobat area (NW of Isfahan, Iran) and its tectonic significance. Journal of Asian Earth Sciences, 37, 207-218.

Mahmoudi, S., Corfu, F., Masoudi, F., Mehrabi, B., Mohajjel, M., 2011. U-Pb dating and emplacement history of granitoid plutons in the Northern Sanandaj-Sirjan zone, Iran. Journal of Asian Earth Sciences,, 41, 238-249.

Masoudi, F., Yardley, B.W.D., Cliff R.A., 2002. Rb-Sr geochronology of pegmatites, plutonic rocks and a hornfels in the region southwest of Arak, Iran. J. Sci., I. R. of Iran, 13 (3): 249-254.

Mohajjel, M., Fergusson, C.L., 2000. Dextral transpression in Late Cretaceous continental collision, Sanandaj-Sirjan Zone, western Iran. Journal of Structural Geology, 22, 1125–1139.

Mohajjel, M., Fergusson C.L., and Sahandi M.R., 2003. Cretaceous-Tertiary convergence and continental collision, Sanandaj-Sirjan Zone, western Iran. Journal of Asian Earth Sciences, 21, 397–412.

Moosavi, E., 2003. Geological Map of the Dehaq Quadrangle, Series 1/100000, No. 6156, Geological Survey of Iran.

Moritz, R., Ghazban, F., Singer, B., 2006. Eocene gold ore formation at Muteh, Sanandaj-Sirjan tectonic zone, western Iran: A result of late-stage extension and exhumation of metamorphic basement rocks within the Zagros Orogen. Economic Geology, 101, 1497–1524.

Neymark, L.A., Amelin, V.Yu., Larin, A.M., 1996. Pb-Nd-Sr isotopic and geochemical constraints on the origin of the 1.54–1.56 Ga Salmi rapakivi granite-anorthosite batholith (Karelia, Russia). Mineralogy and Petrology, 50, 1-3, 173-193.

Nezafati, N., Herzig, P.M., Pernicka, E., Momenzadeh, M., 2005. Intrusion-related gold occurrences in the Astaneh-Sarband area, west central Iran. Mineral Deposit Research Meeting: The Global Challenge.

NIOC (National Iranian Oil Company), 1975. Geological Map of Iran, Scale 1/1000000. Sheet No. 3-4, Northwest and Southwest Iran.

Paces, J.B., Miller, J.D., 1993. Precise U-Pb age of Duluth Complex and related mafic intrusions, northeastern Minnesota: Geochronological insights into physical, petrogenic, paleomagnetic, and tectonomagnetic processes associated with the 1.1 Ga mid-continent rift system, Journal of Geophysical Research, 98, 13,997–14,013.

Pearce, J.A., Harris, N.B.W., Tindle, A.G., 1984. Trace element discrimination diagrams for the tectonic interpretation of granitic rocks. J. Petrol, 25: 956-983.

Quidelleur, X.M., Grove, O.M. Lovera, T. M. Harrison, A. Yin, and Ryerson, F.J., 1997. Thermal evolution and slip history of the Renbu Zedong thrust, southeastern Tibet, Journal of Geophysical Research, 102, 2659–2679.

Rachidnejad-Omran, N., Emami, M.H., Sabzehi, M., Rastad, E., Belon, H., Pique, A., 2002. Lithostratigraphie et histoire paléozoïque à Paléocène des complexes métamorphiques de la région de Muteh, zone de Sanandaj–Sirjan (Iran méridional). Comptes Rendus Geosciences 334, 1185–1191.

Rämö O.T., Dall'Agnol, R., Macambira M.J.B., Leite A.A.S., de Oliveira D.C. (2002) 1.88 Ga oxidized A-type granites of the Rio Maria Region, Eastern Amazonian Craton, Brazil, positively Anorogenic. The Journal of Geology, 110, 603-610.

Rämö, O.T., Frindt, S., 2005. Comparison of Proterozoic and Phanerozoic rift-related basaltic-granitic magmatism. Lithos, 80, 1-4, 1-32.

Robertson, A.H.F., Parlak, O., Rízaoğlu, T., Ünlügenç Ü., İnan, N., Tasli, K., Ustaömer, T., 2007. Tectonic evolution of the South Tethyan Ocean: evidence from the Eastern Taurus Mountains (Elaziğ region, SE Turkey) The Geological Society of London, 272: 231-270.

Schmitt, A.K., Grove, M., Harrison, T.M., Lovera, O.M., Hulen, J., Waters, M., 2003a. The Geysers-Cobb Mountain Magma System, California (Part 1): U-Pb zircon ages of volcanic

rocks, conditions of zircon crystallization and magma residence times, Geochimica et Cosmchimica Acta, 67, 3423–3442.

Schmitt, A.K., Grove, M., Harrison, T.M., Lovera, O.M., Hulen, J., Waters, M., 2003b. The Geysers-Cobb Mountain Magma System, California (Part 2): Timescales of pluton emplacement and implications for its thermal history, Geochimica et Cosmchimica Acta, 67, 3443–3458.

Sepahi, A.A., Athari, S.F., 2006. Petrology of major granitic plutons of the northwestern part of the Sanandaj-Sirjan Metamorphic Belt, Zagros Orogen, Iran: with emphasis on A-type granitoids from the SE Saqqez area. N. Jb. Miner. Abh. 183/1, 93–106.

Shahbazi, H., Siebel, W., Pourmoafee, M., Ghorbani, M., Sepahi, A.A., Shang, C.K., Vosoughi Abedini, M., 2010. Geochemistry and U-Pb zircon geochronology of the Alvand plutonic complex in Sanandaj-Sirjan Zone (Iran): New evidence for Jurassic magmatism. Journal of Asian Earth Sciences, 9, 668-683.

Stacey, J.S., and J.D. Kramers, 1975. Approximation of terrestrial lead isotope evolution by a two stage model, Earth and Planetary Science Letters, 26, 207–221.

Stöcklin, J., 1968. Structural history and tectonics of Iran: A review: American Association of Petroleum Geologists Bulletin, 52, 1229–1258.

Stöcklin, J., Setudehnia, A., 1970. Stratigraphic Lexicon of Iran. Geological Survey of Iran, Tehran, Iran.

Streckeisen, A., Le Maitre, R.W., 1979. A chemical approach to the modal QAPF classification of the igneous rocks. N. Jb. Miner. Abh. 136, 2, 169-206.

Stull, R.J., 1973. Calcic and alkali amphiboles from the Golden Horn batholith, north Cascades, Washington. American Mineralogist, 58, 873-878.

Sun, S.S., McDonough, W.F., 1989. Chemical and isotopic systematics of oceanic basalts: implications for mantle composition and processes. In: Sunders, A.D., Norry, M.J. (Eds.) Magmatism in the Ocean Basins, vol. 42. Geological Society Special Publications, London, 313–345.

Thiele, O., Alavi, M., Assefi, R., Hushmandzadeh, A., Seyed-Emami, K., Zahedi, M., 1968. Explanatory text of the Golpaygan quadrangle map. Geological Survey of Iran, Tehran, Iran.

Tillman, J.E., Poosti, A., Rossello, S., and Eckert, A., 1981, Structural evolution of Sanandaj-Sirjan Ranges near Esfahan, Iran: American Association of Petroleum Geologists Bulletin, v. 65, p. 674–687.

Vail, J.R., 1985. Alkaline ring complexes in Sudan. In: Black, R., and Bowden, P. (eds), Alkaline Ring Complexes in Africa. J. Afr. Earth Sci., 3, pp. 51–59.

Watson, E.B., Harrison, T.M., 1983. Zircon Saturation revisited. EPSL 64, 295-304.

Whalen, J.B., Currie, K.L., Chappell B.W., 1987. A-type granites: geochemical characteristics, discrimination and petrogenesis. Contrib. Mineral. Petrol., 95, 407-419.

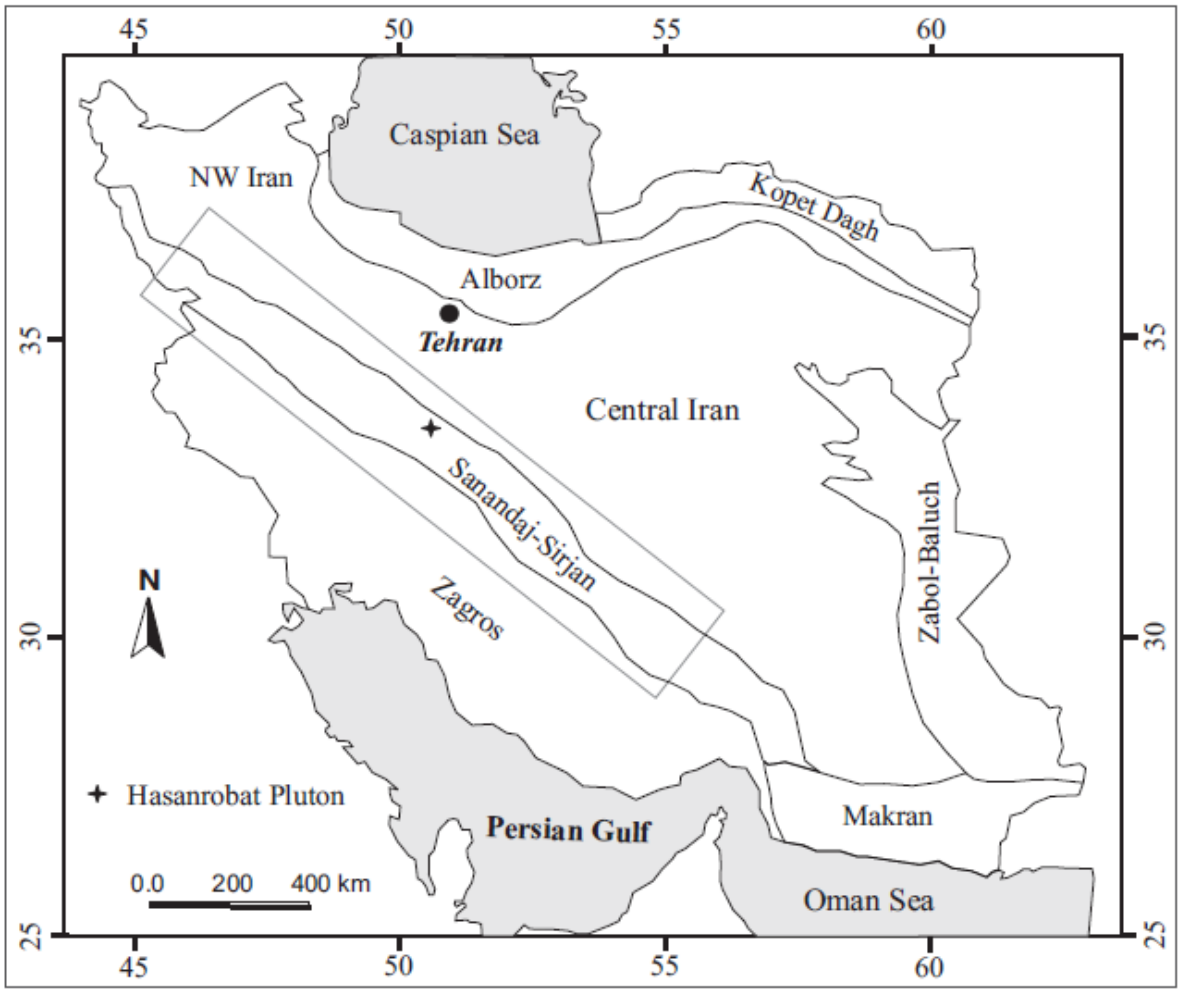

Fig. 1

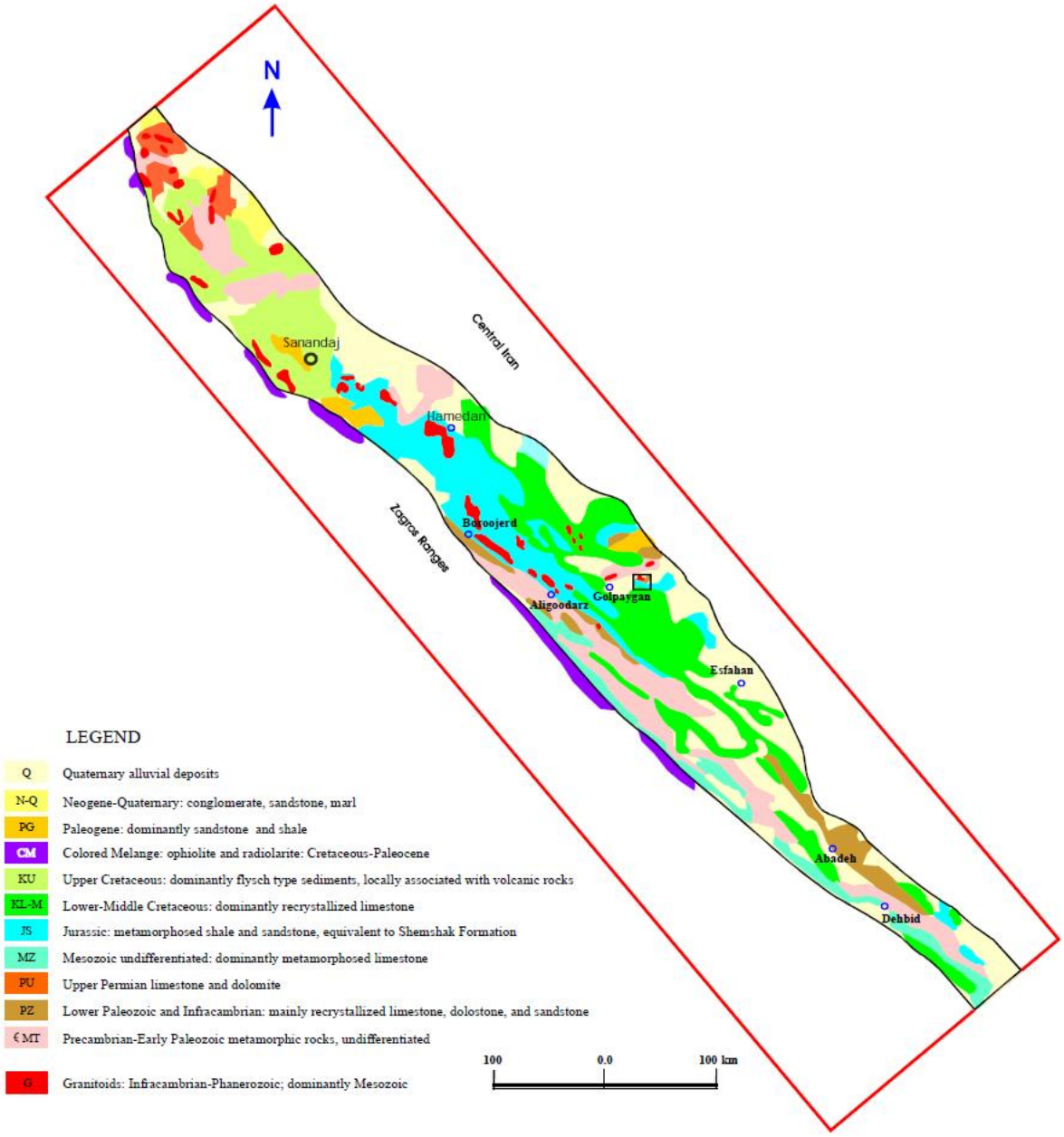

Fig. 2

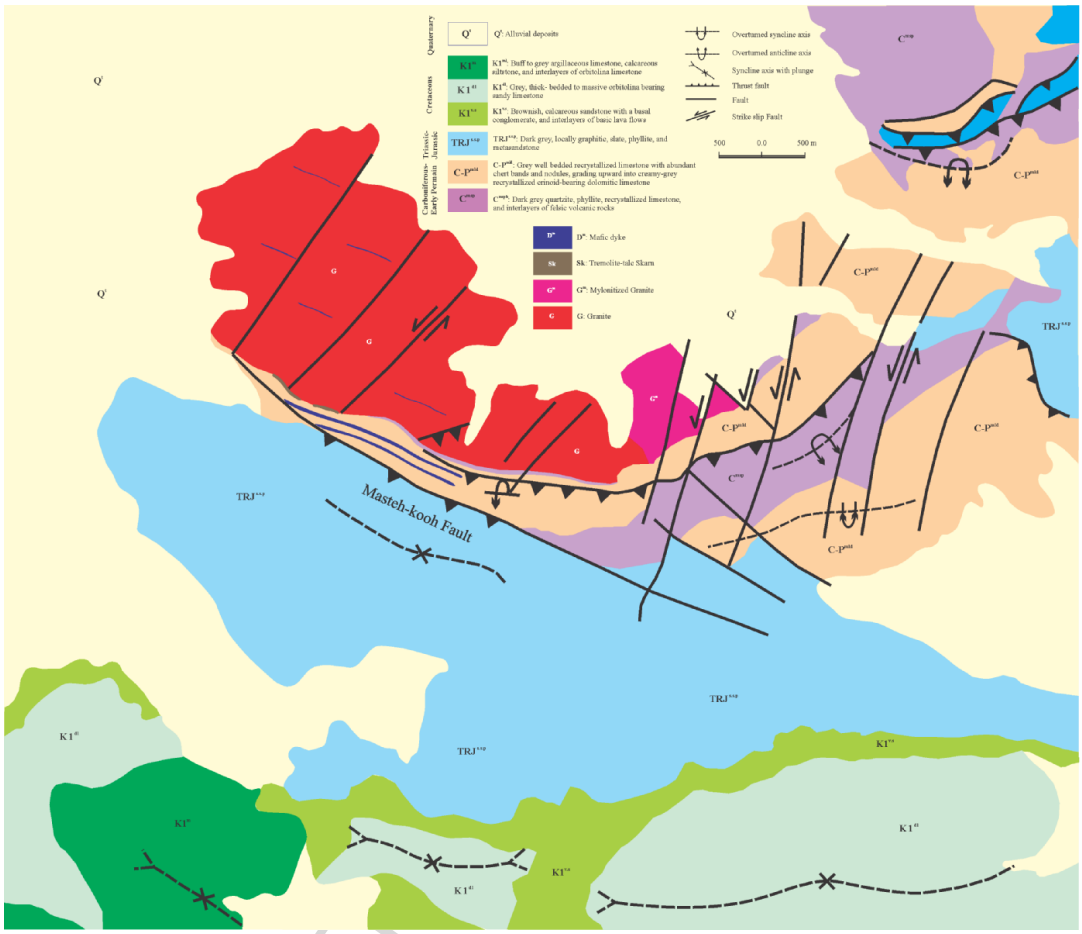

Fig. 3

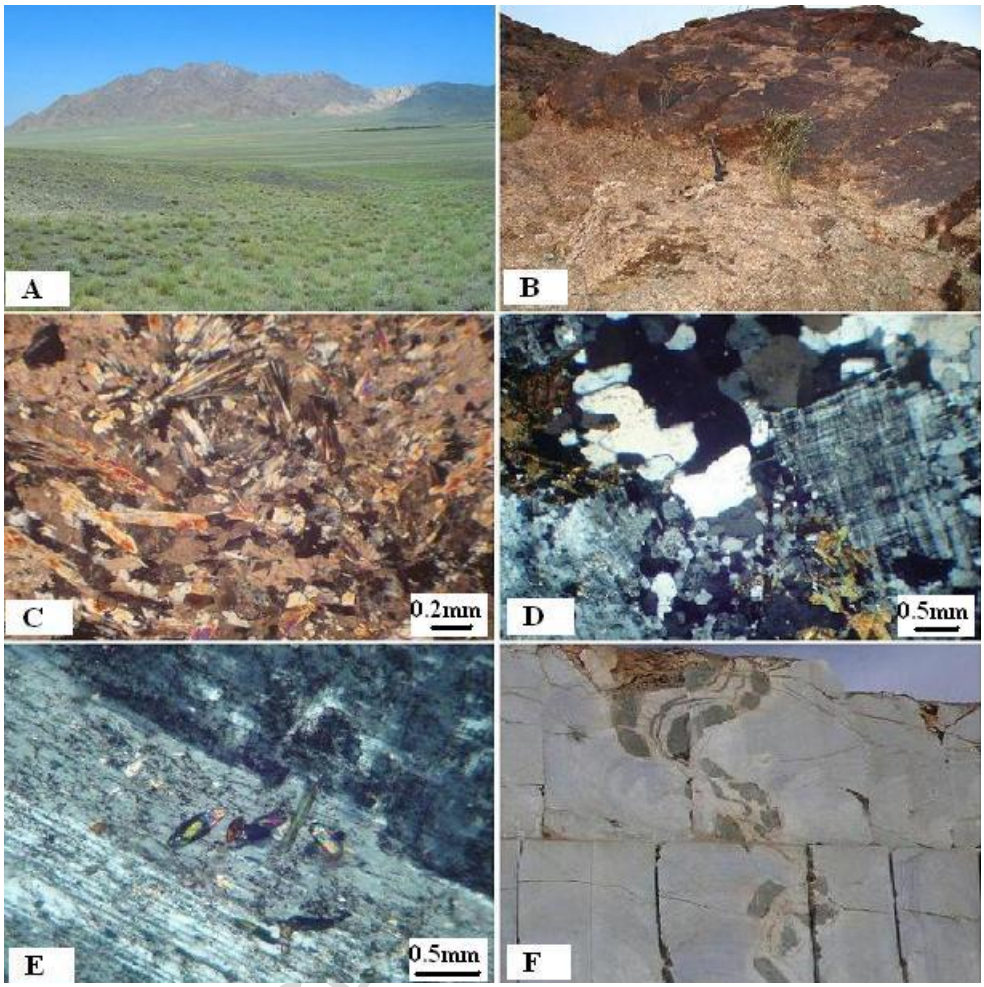

Fig. 4

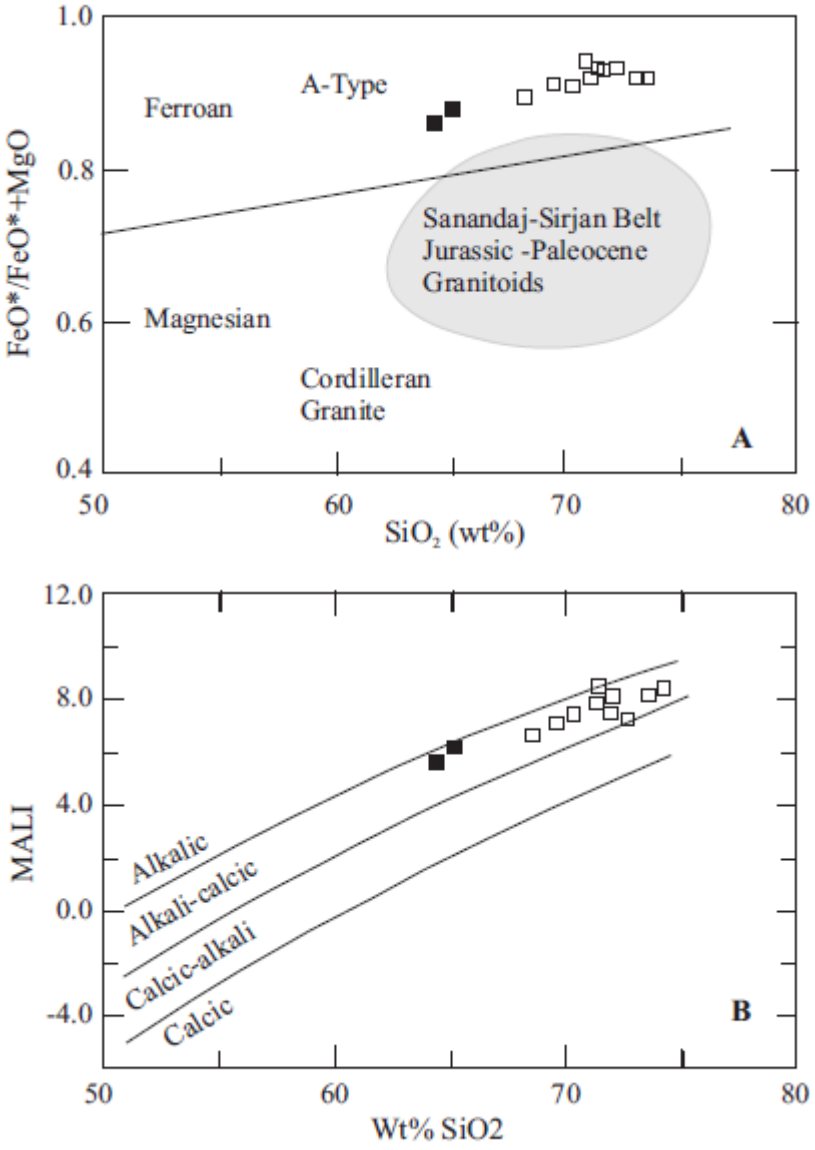

Fig. 5

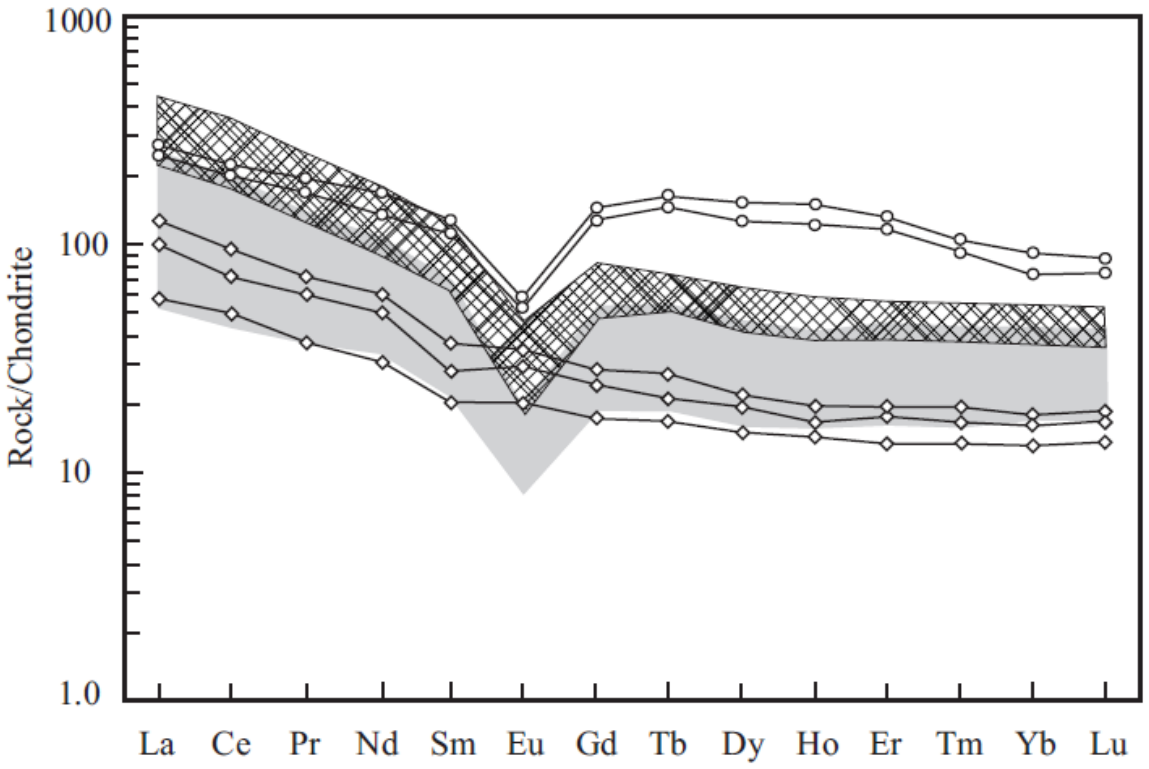

Fig. 6

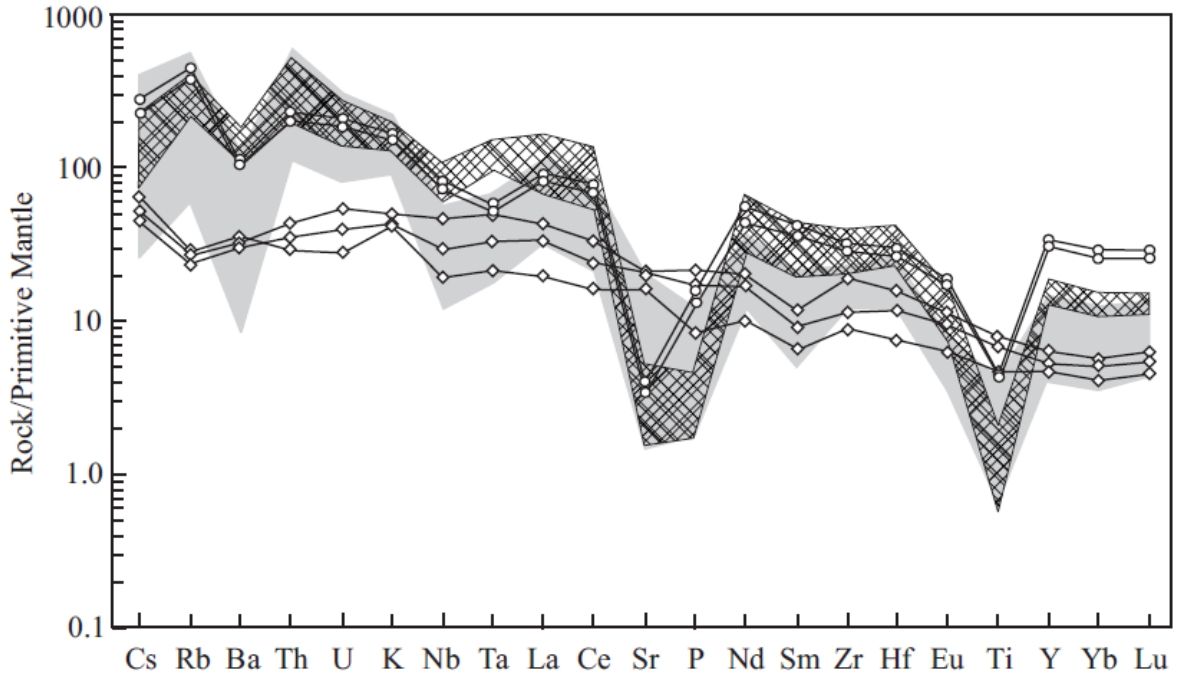

Fig. 7

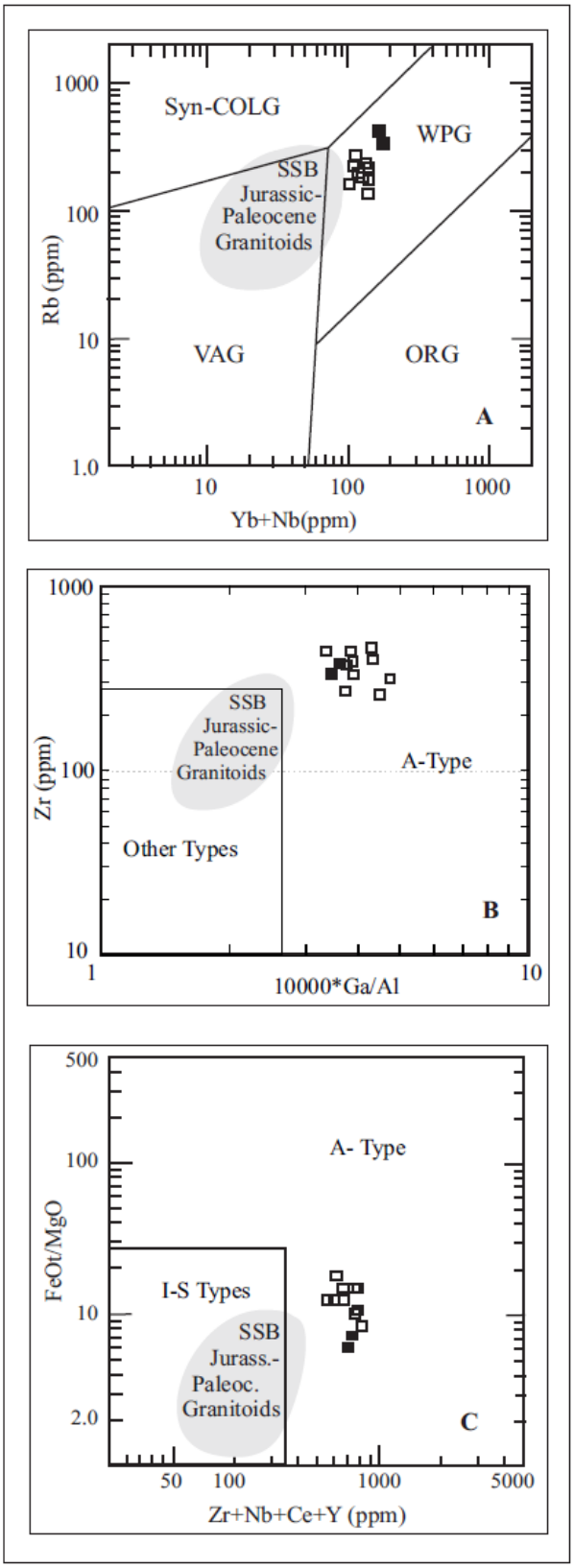

Fig. 8

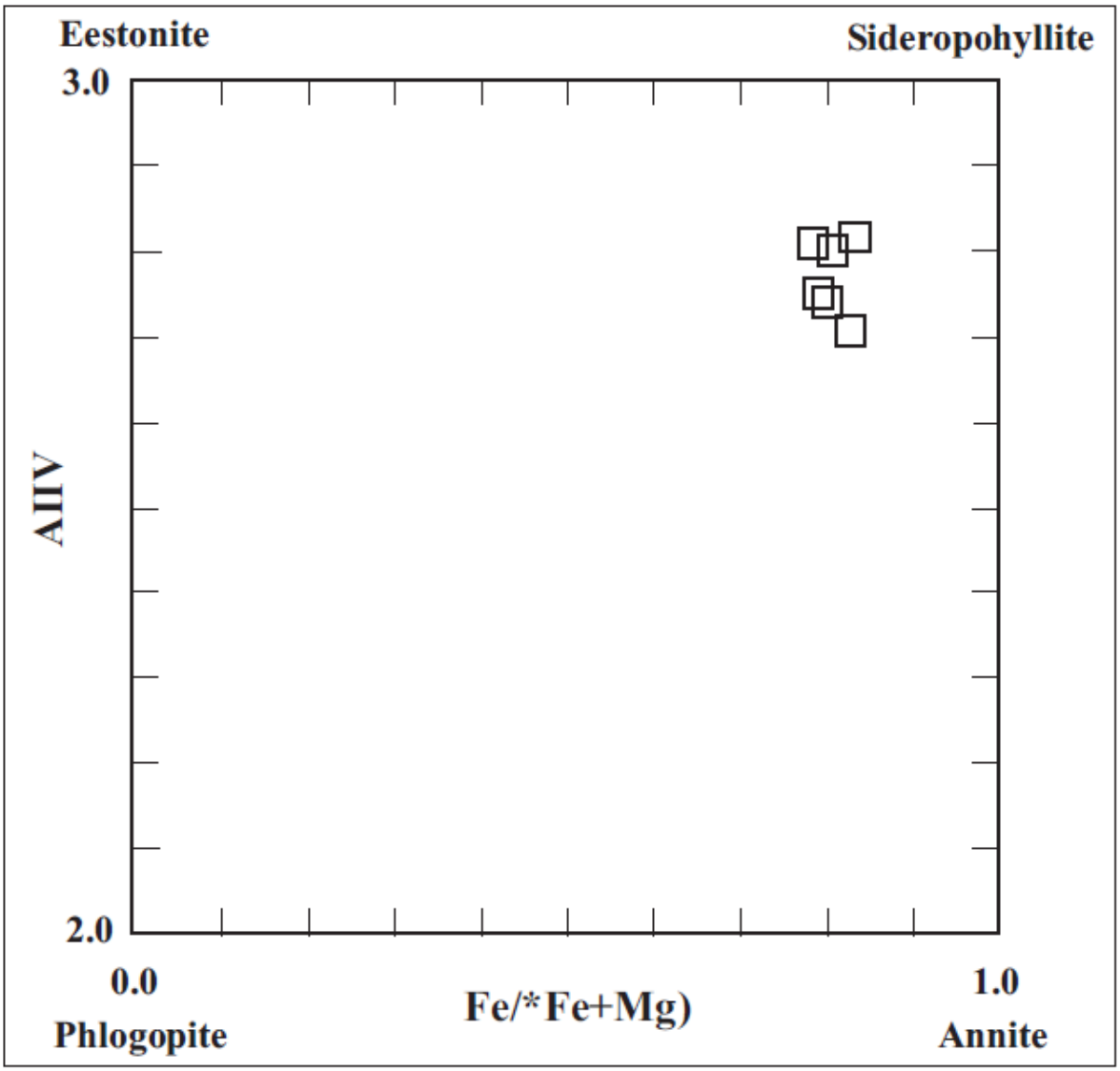

Fig. 9

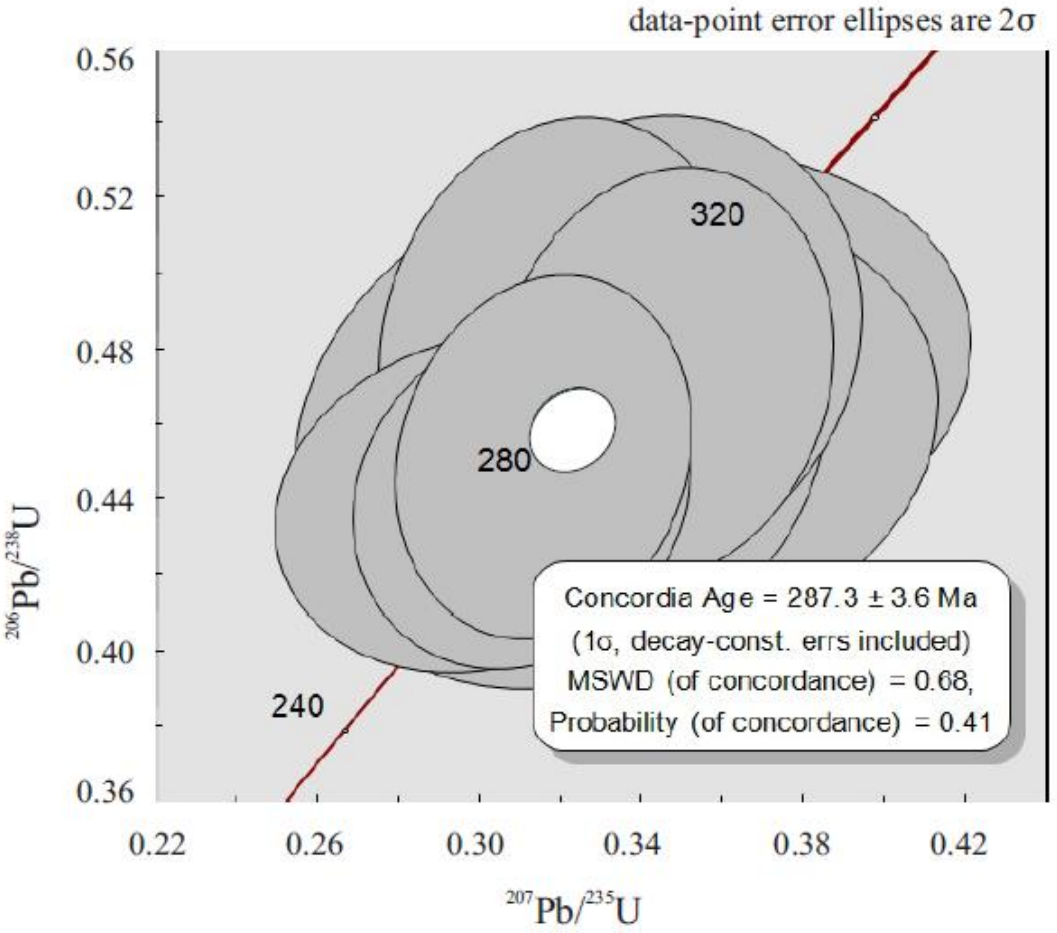

Fig. 10

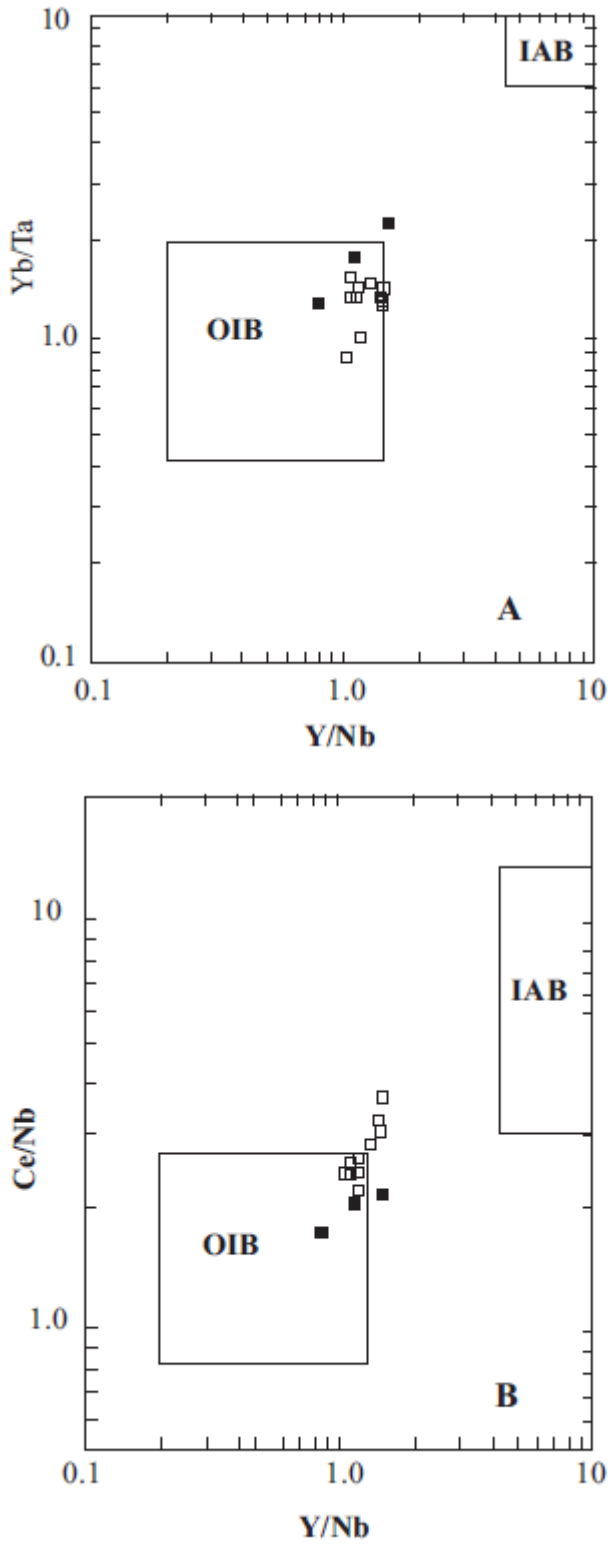

Fig. 11

Appendix 1.															
05HSR					Correlation	Age (Ma)	Age (Ma)	% Radiogenic	Age (Ma)	Age (Ma)	% Radiogenic	Age (Ma)	Age (Ma)	U (ppm)	Th (ppm)
	207Pb*/	207Pb*/	206Pb*/	206Pb*/	of Concordia	206Pb/	206Pb/	206Pb	207Pb/	207Pb/	207Pb	207Pb/	207Pb/		
	235U	235U	238U	238U	Ellipses	238U	238U		235U	235U		206Pb	206Pb		
Grain ID		1 s.e.		1 s.e.			1 s.e.			1 s.e.			1 s.e.		
5	0.31950	0.01812	0.04841	0.00237	0.826	304.7	14.6	99.6	281.6	13.9	92.8	93.22	75.8	5473	2166
4	0.33930	0.02258	0.04808	0.00252	0.775	302.7	15.5	99.5	296.7	17.1	92.7	249.2	96.8	2836	785
1	0.34340	0.03190	0.04738	0.00240	0.547	298.4	14.8	98.2	299.7	24.1	77.2	310.1	177	2463	638
3	0.34560	0.01720	0.04736	0.00225	0.902	298.3	13.8	99.7	301.4	13	95.3	325.5	49	5888	2318
6	0.34050	0.02989	0.04580	0.00247	0.783	288.7	15.2	99.6	297.6	22.6	94.2	367.8	128	1195	310
2	0.32010	0.02683	0.04576	0.00274	0.765	288.4	16.9	99.4	282	20.6	91.3	228.5	125	1839	550
7	0.31560	0.01497	0.04521	0.00197	0.933	285	12.2	100	278.5	11.6	99.2	224.3	39.4	9860	3093
8	0.31030	0.01707	0.04416	0.00188	0.837	278.5	11.6	99.5	274.4	13.2	92.2	239.6	69.9	5128	1720
9	0.30020	0.02076	0.04396	0.00184	0.662	277.4	11.3	99.5	266.6	16.2	91.6	172.8	121	2476	1273
Weighted mean $^{206}Pb/^{238}U$ age = 288.3 ± 3.6 Ma, MSWD = 0.86, probability = 0.35															
Not used in calculations															
10	0.23570	0.01945	0.03685	0.00172	0.666	233.3	10.7	98.6	214.9	16	80.3	18.07	149	3133	766

Table 1. Chemical analysis of the Hasanrobat granite, biotite-rich enclaves and mafic dykes

						Granite					Biot.-rich encl.		Mafic Dyke		
	HR-03	HR-05	HR-08A	HR-11	HR-12	05HSR	HR-10A	HR-10B	HR-102	HR-115	HR-110	HR-120	HR-111	HR-112	HR-301
SiO2(%)	73.64	71.14	69.40	68.15	70.23	71.18	71.53	72.27	71.68	73.14	65.05	64.15	48.35	49.32	48.56
TiO2	0.17	0.28	0.45	0.52	0.33	0.24	0.30	0.28	0.24	0.19	1.00	1.13	1.53	1.78	1.06
Al2O3	13.33	13.7	13.72	14.37	14.18	14.06	13.43	13.29	14.10	13.42	13.93	13.82	16.75	17.20	17.14
Fe2O3	2.01	3.27	4.59	4.83	3.81	2.88	3.27	3.12	2.78	2.24	7.32	7.96	11.05	10.40	9.98
MnO	0.03	0.05	0.08	0.09	0.06	0.04	0.05	0.05	0.04	0.04	0.13	0.17	0.15	0.13	0.16
MgO	0.18	0.29	0.45	0.58	0.39	0.18	0.24	0.23	0.21	0.20	1.00	1.28	5.65	5.08	6.99
CaO	0.66	1.21	1.52	1.59	1.11	1.00	1.30	1.26	0.90	0.79	1.91	2.05	8.96	8.32	8.54
Na2O	3.53	3.75	3.52	3.71	3.55	3.72	4.13	3.71	3.69	3.81	3.07	2.95	4.28	4.51	3.12
K2O	5.41	5.36	5.04	4.69	5.15	5.75	4.67	4.72	5.35	5.28	5.17	4.82	1.34	1.51	1.29
P2O5	0.05	0.06	0.13	0.14	0.11	0.042	0.07	0.07	0.05	0.05	0.30	0.35	0.39	0.48	0.19
LOI	0.90	0.70	0.90	0.95	0.80	0.7	0.80	0.70	0.70	0.65	0.80	0.85	1.10	0.90	2.60
Total	99.91	99.81	99.80	99.62	99.72	99.79	99.79	99.70	99.74	99.81	99.68	99.53	99.55	99.63	99.63
Rb (ppm)	222	182	196	166	208	175	191	191	218	235	294	277	15.5	18.2	18.8
Cs	2.90	3.90	6.10	5.85	5.40	3.6	4.50	4.10	3.80	3.20	9.10	8.80	1.60	1.70	2.10
Ba	615	1006	1117	1165	1054	836	786	805	850	718	782	794	217	238	254
Sr	44	66	97	112	91	61	75	71	66	53	75	83	453	472	356
Ta	6.6	4.7	4.9	4.5	5.1	4.2	5.4	4.9	4.6	7.2	2.5	2.3	1.40	2.10	0.90
Th	37.2	19.9	17.4	15.4	15.9	17.9	22.8	21.7	23.4	29.6	20.5	18.7	3.05	3.90	2.50
U	5.2	3.7	3.8	3.2	4.0	3.1	4.4	4.2	3.3	5.4	4.6	4.3	0.9	1.2	0.6
Be	7.0	6.0	4.0	3.0	4.0	5.0	8.0	5.0	6.0	9.0	6.0	5.0	2.0	2.0	<1
La	62	77	82	86	86	76	96	101	79	69	65	59	23.7	30.4	13.9
Ce	131	160	172	178	183	149	198	210	154	152	140	125	44.2	59.6	30.2
Pr	13.9	17.3	18.9	20.3	19.7	17.7	21.1	22.1	18.3	14.8	18.6	15.8	5.7	7.0	3.5
Nd	48.7	61.8	71.2	69.8	75.5	65.9	77.0	76.0	70.8	57.8	77.6	63.2	23.9	28.3	14.2
Sm	11.0	13.1	15.5	14.9	15.6	12.8	16.8	16.6	13.2	12.4	19.2	16.9	4.15	5.5	3.04
Eu	1.23	1.81	2.37	2.68	2.14	1.77	1.72	1.85	1.86	1.38	3.28	3.12	1.64	1.97	1.15
Gd	10.9	12.7	13.2	12.9	13.6	10.6	15.6	15.0	12.7	11.2	28.5	25.6	4.85	5.74	3.43
Tb	1.98	2.11	2.41	2.26	2.42	2.09	2.51	2.46	2.17	2.05	5.94	5.25	0.78	0.98	0.61
Dy	11.1	11.9	12.5	13.2	12.6	11.8	14.9	14.6	12.3	11.8	37.6	31.8	4.82	5.35	3.68
Ho	2.37	2.48	2.60	2.84	2.74	2.45	3.01	2.67	2.47	2.28	8.19	6.76	0.92	1.09	0.79
Er	7.45	7.29	7.54	8.12	7.32	7.28	8.18	7.89	7.16	7.42	21.06	18.7	2.85	3.18	2.18
Tm	1.14	1.12	1.23	1.15	1.19	1.13	1.28	1.11	1.10	1.08	2.66	2.48	0.42	0.49	0.34
Yb	7.28	7.03	6.93	7.28	7.12	6.49	7.48	7.32	6.57	7.05	14.76	13.35	2.59	2.89	2.13
Lu	1.12	1.06	1.05	1.10	1.03	0.98	1.09	1.15	1.00	1.18	2.18	2.05	0.42	0.47	0.34
Ni	1.0	1.3	2.3	4.2	1.10	1.9	1.3	3.3	3.10	0.08	4.3	5.8	34.5	29.7	55.0
Sc	5.0	12.0	14.0	13.0	12.0	9.0	12.0	11.0	10.0	7.0	14.0	17.0	33.0	29.0	28.0
Co	0.8	1.3	2.8	3.2	2.7	1.4	1.6	2.0	1.4	0.7	9.3	10.2	33.4	28.2	37.9
Cr	34	118	105	133	112	105	56	20	39	24	80	87	173	116	191
Ga	31	27	28	32	25	28	30	27	29	34	27	26	21	19	17
Hf	9.1	11.0	11.3	13.1	11.8	9.3	11.0	11.3	10.0	9.5	9.5	8.8	3.8	4.9	2.4
Nb	61	62	66	73	58	50	59	55	64	63	61	56	21.5	34.5	14.0
V	<5	6.0	18	23	12	<5	9.0	9.0	<5	<5	77	88	213	185	188
W	1.5	7.0	7.7	7	6.00	1.7	3.9	4.8	7.90	2.50	7.7	5.2	1.00	4.30	0.60
Zr	265	368	430	454	413	309	393	376	336	316	369	345	135	215	103
Y	74	73	75	82	83	66	85	81	74	69	148	152	24.8	29.8	21.5
Mo	0.2	0.4	0.5	1.0	0.7	0.5	0.4	1.4	1.6	0.4	1.0	1.0	0.50	2.80	0.20
Cu	2.1	2.6	2.4	4.1	2.0	4.6	1.6	3.3	2.4	2.8	2.3	3.8	41.6	42.0	37.8
Sn	10.0	7.0	10.0	8.0	7.0	7.0	5.0	4.0	5.0	8.0	16.0	12.0	2.0	2.0	2.0
Pb	12.6	7.0	7.4	7.65	8.20	11.4	6.1	20.1	7.10	11.50	5.3	5.5	10.8	3.5	20.0
Zn	69	85	178	215	134	92	87	87	91	73	360	344	62	58	48
As	2.5	1.0	1.0	1.0	1.0	2.1	1.4	1.5	<0.5	2.0	0.7	0.5	1.5	1.7	13.1
Cd	0.2	0.2	0.2	0.3	0.10	0.1	0.1	<0.1	<0.1	0.2	0.30	0.35	0.20	0.20	0.40
Sb	0.1	0.1	0.1	0.1	0.1	0.2	0.1	0.1	<0.1	0.1	<0.1	<0.1	0.10	0.20	0.20
Bi	0.2	0.1	0.1	0.2	0.1	0.1	0.3	0.3	2.10	0.30	<0.1	<0.1	<0.1	<0.1	<0.1
Au	1.5	<.5	0.7	0.7	1.2	<0.5	1.1	0.8	<.5	0.6	1.5	1.5	2.0	1.0	1.0
Tl	0.4	0.4	0.5	0.5	0.60	0.3	0.4	0.4	0.10	0.20	1.0	1.0	0.20	0.10	<0.1

Table 2. Electron microprobe analysis of selected minerals for Hasanroabat granite

	Biotite (7)*		Aphibole (9)		Plagioclase (4)		Microcline (2)
	Mean	1σ	Mean	1σ	Mean	1σ	Mean
SiO2	35.73	0.50	37.63	0.24	67.09	2.16	65.78
TiO2	2.58	0.56	0.37	0.05	0.00	0.00	0.00
Al2O3	16.24	0.52	13.48	0.28	20.78	1.61	18.21
Cr2O3	0.01	0.02	0.03	0.02	–	–	–
FeO**	27.52	1.03	29.15	0.16	0.03	0.02	0.08
MnO	0.51	0.11	0.77	0.02	–	–	–
MgO	3.70	0.30	1.98	0.09	–	–	–
BaO	0.22	0.34	–	–	–	–	0.33
CaO	0.03	0.04	11.15	0.07	1.89	1.85	0.00
Na2O	0.05	0.03	1.26	0.06	10.64	1.00	0.52
K2O	9.13	0.36	2.08	0.05	0.09	0.03	15.30
F	1.03	0.33	NA***	NA	–	–	–
Cl	0.15	0.02	NA	NA	–	–	–
H2O calc.	3.62	0.07	NA	NA	–	–	–
OH_F_Cl	0.47	0.14	–	–	–	–	–
Total	100.06	1.22	97.90	0.48	100.51	0.33	100.21

* number of analyses; ** all Fe reported as FeO; *** not analyzed

Highlights

- This is the first documentation of an A-type granite of Upper Paleozoic age in Sanandaj-Sirjan Belt (SSB) of Iran.
- The Hasanrobat granite stands distinct from many other, dominantly Mesozoic, I-type, granitoids in SSB by its A-type nature.
- The zircon U-Pb age of the granite (289 ± 5 Ma) corresponds to a rifting episode in Lower Permian in northern Gondwana.
- Our findings strengthen an earlier view, based on stratigraphy, for a Permian timing for the opening of Neotethys in Iran.
- Our findings further support the view that many A-type granites form in rift settings in the course of continental break-up.